Asia Pacific Science Press

Asia Pacific Economic and Management Review
ISSN(O):3005-9275
ISSN(P):3005-9267
Vol. 3 No.2 (2026)

A Bilevel GA–PSO–MILP Framework for Capacity Planning and Day-Ahead Scheduling of an Integrated Electricity–Heat–Cooling Energy System

Mengzhe Yu[1], Mingshen Xu[1]*, Bomian Cheng[2]

1. North China Electric Power University, Baoding, Hebei, 071003, China
2. Chengdu University of Technology, Chengdu, Sichuan, 610059, China

Corresponding author: Mingshen Xu, 3165865378@qq.com

Abstract: This paper proposes a bilevel planning–operation framework for an integrated electricity–heat– cooling energy system comprising photovoltaic generation, wind generation, a gas-turbine-based combined heat and power unit, a ground source heat pump, a gas boiler, battery storage, thermal storage, an absorption chiller, and an electric chiller. The upper level determines the installed capacities of major devices, while the lower level performs day-ahead coordinated dispatch over four representative days. To preserve the engineering logic of the original optimization program while improving analytical transparency and reproducibility, the planning layer is formulated as a GA–PSO-based search procedure and the coupled planning–operation problem is further expressed as an equivalent mixed-integer linear benchmark model. A complete mathematical formulation is provided, including explicit decision-variable definitions, energy-conversion relationships, storage dynamics, logical constraints, and a comprehensive notation table. Using the representative-day data embedded in the program package, the optimal configuration is obtained as 800 kWh battery storage, 900 kW photovoltaic, 600 kW wind, 1200 kW gas turbine, 300 kW ground source heat pump, 200 kW gas boiler, 600 kWh thermal storage, 479.08 kW absorption chiller, and 150 kW electric chiller. The corresponding daily equivalent annualized investment cost is 6286.79, the day-ahead composite operating objective is 77400.43, and the ex-post composite operating objective under realized loads is 78763.31. The results indicate that strong renewable deployment, flexible storage scheduling, and coordinated electricity–heat–cooling conversion can substantially improve the economic and operational performance of integrated energy systems.

Keywords: Integrated Energy System; Bilevel Optimization; Capacity Planning; Day-Ahead Scheduling; GA–PSO; Mixed-Integer Linear Programming

Published: Apr 7, 2026

DOI: https://doi.org/10.62177/apemr.v3i2.1229

1. Introduction

Integrated energy systems provide a physically coupled platform for the coordinated production, conversion, storage, and utilization of multiple energy carriers, including electricity, heat, cooling, and gas. By exploiting complementary interactions among different conversion devices and demand types, such systems can improve renewable-energy utilization, reduce operating cost, and enhance local energy flexibility. Energy hub theory established the conceptual basis for multi-carrier coordination [1-2], and subsequent studies on distributed multi-generation, building energy systems, and multi-energy micro-

grids gradually extended this concept toward practical planning and operation problems [3-5]. At broader spatial scales, integrated electricity–heat–gas and electricity–heat–cooling systems have been studied from infrastructure, planning, dispatch, and policy perspectives [6-9].

Recent research has increasingly focused on more detailed planning and operational models for integrated energy systems. Optimization frameworks have been proposed to represent technology coupling, demand response, infrastructure interaction, and uncertainty across different carriers [10-12]. Two-stage, robust, and decomposition-based methods have improved the treatment of uncertain loads and renewable availability [13-14]. In parallel, resilience-oriented planning, carbon-aware expansion, and integrated electricity–heat design methods have further enriched the methodological landscape [15-18].

Despite these advances, two practical issues remain common in engineering-oriented studies. First, the planning layer and the operational layer are often described only at a conceptual level, which makes it difficult to identify the exact coupling between investment decisions and day-ahead dispatch. Second, program-based implementations frequently contain complete computational logic but insufficient mathematical exposition, especially regarding notation, logical constraints, and equivalent linear reformulations.

For upper-level capacity planning, heuristic search remains attractive because the capacity mix of integrated energy systems is affected by nonconvex equipment interactions, long-term investment trade-offs, and feedback from lower-level operation. The methodological roots of this approach can be traced to genetic algorithms and evolutionary search [19], as well as particle swarm optimization [20]. For lower-level coordinated dispatch, algebraic modeling platforms and commercial mixed-integer optimization solvers are widely used because they can efficiently handle time-coupled scheduling constraints and logical operating states [21-22]. The optimization code supporting this study follows exactly this combination: a GA–PSO planning layer is coupled with a YALMIP–GUROBI operational dispatch model over four representative days.

Motivated by the need for a more rigorous and publication-ready presentation, this paper reorganizes the original engineering model into a complete bilevel planning–operation manuscript. The contribution of the paper is fourfold. First, the coupled electricity, heat, cooling, gas, and storage interactions are systematically reformulated as a bilevel capacity-planning and day-ahead scheduling model. Second, the upper-level GA–PSO search philosophy is retained, while the full planning–operation linkage is further rewritten as an equivalent mixed-integer linear benchmark model to improve reproducibility and analytical clarity. Third, a unified notation system and explicit parameter specification are provided to eliminate ambiguity in variables and constraints. Fourth, the numerical case study interprets the optimal capacity mix and the representative-day dispatch behavior from the perspective of renewable integration, CHP-led coupling, storage flexibility, and dual cooling technologies.

The remainder of this paper is organized as follows. Section 2 introduces the integrated electricity– heat–cooling system and the bilevel decision structure. Section 3 presents the complete mathematical formulation. Section 4 describes the solution methodology, including the GA–PSO procedure and the exact MILP benchmark reformulation. Section 5 reports the case-study settings, and Section 6 discusses the numerical results. Section 7 concludes the paper.

2. System Description and Problem Statement

2.1 Integrated Electricity–Heat–Cooling System Architecture

The system considered in this paper contains three tightly coupled demand categories: electricity demand, heat demand, and cooling demand. The electricity subsystem consists of photovoltaic generation, wind generation, the electric output of a gas-turbine-based combined heat and power (CHP) unit, battery storage, the electrical input of the ground source heat pump, the electrical input of the electric chiller, and bidirectional power exchange with the external grid. The heat subsystem consists of CHP thermal recovery, the heat supplied by the ground source heat pump, a gas boiler, thermal storage, and the heat consumed by the absorption chiller. The cooling subsystem is jointly served by the electric chiller and the absorption chiller. Natural gas is purchased from the external gas network and is consumed by the CHP unit and the gas boiler.

The operational scheduling horizon is 24 hours for each representative day. Long-term planning is reflected through daily equivalent annualized investment costs. Let d denote the representative-day index and t the hourly index. The upper level determines the installed capacity vector

$$X = [X_{es}, X_{pv}, X_{wt}, X_{gt}, X_{hp}, X_{gb}, X_{hs}, X_{ac}, X_{ec}]^{T}. \quad (1)$$

where each element represents the installed size of a major technology. Given X, the lower level optimizes the day-ahead dispatch of all energy carriers and controllable devices.

2.2 Bilevel Planning–Operation Structure

The interaction between planning and operation is depicted by a master–subproblem structure. The upper level selects device capacities by balancing capital expenditure against the operating performance induced by those capacities. The lower level receives a fixed capacity vector and schedules the system over each representative day so as to minimize a composite operating objective that includes direct cost and environmental penalty. This structure can be written compactly as

$$\min_{X\in X} F(X) = C^{inv}(X) + \sum_{d=1}^{4} \omega_d \Phi_d(X) \tag{2}$$

where X denotes the feasible planning set, wd is the weight of representative day d, cinv is the daily equivalent annualized investment cost, and Φd(X) is the optimal lower-level objective value correspond- ing to representative day d. In the present case study, all representative-day weights are set to one, consistent with the aggregation logic adopted in the optimization code.

For a fixed capacity vector X, the lower-level problem on representative day d is

$$\Phi_d(X) = \min_{y_d \in Y_d(X)} \left(C_d^{dir} + C_d^{em}\right) \tag{3}$$

where yd collects all operational decision variables and Yd(X) denotes the day-ahead feasible region induced by energy-balance equations, conversion relationships, storage dynamics, logical operating states, and device-capacity limits.

3. Mathematical Formulation

3.1 Upper-Level Planning Model

The admissible range of each planning variable is

$$X_j \le X_j \le X_j, \ \forall j \in \{es, pv, wt, gt, hp, gb, hs, ac, ec\} \tag{4}$$

where xj and x j are the lower and upper capacity bounds, respectively. The daily equivalent annualized investment cost is calculated through the capital recovery factor:

$$CRF_j = \frac{r(1+r)^{L_j}}{(1+r)^{L_j}-1} \tag{5}$$

$$C^{inv}(X) = \frac{1}{365}\sum_j CR\, F_j c_j^{cap} X_j \tag{6}$$

where r is the discount rate, Lj is the service life of technology j, and c_j^{cap} is the unit capital cost.

Equation (6) maps long-term investment into an equivalent daily cost so that it can be aggregated with representative-day operating terms in the upper-level objective (2).

3.2 Lower-Level Direct Operating Objective

For representative day d, the direct operating expenditure consists of electricity trading cost, gas purchase cost, and variable operation and maintenance cost:

$$\begin{aligned} C_d^{dir} = {} & \sum_{t=1}^{24} \lambda_{d,t}^{e}\left(p_{d,t}^{buy} - p_{d,t}^{sell}\right) + \sum_{t=1}^{24} \lambda_{d,t}^{g} g_{d,t}^{buy} \\ & + \sum_{t=1}^{24}\left[c_{pv}^{om} p_{d,t}^{pv} + c_{wt}^{om} p_{d,t}^{wt} + c_{gt}^{om} p_{d,t}^{gt} + c_{es}^{om}\left(p_{d,t}^{ch} + P_{d,t}^{dis}\right)\right] \\ & + c_{hp}^{om}\, p_{d,t} + c_{gb}^{om} h_{d,t}^{gb} + c_{hs}^{om}\left(h_{d,t}^{ch} + h_{d,t}^{dis}\right) + c_{ac}^{om} c_{d,t}^{ac} + c_{ec}^{om} p_{d,t}^{ec} \end{aligned} \tag{7}$$

In addition to direct expenditure, the model includes an environmental penalty term:

$$C_d^{em} = \sum_{t=1}^{24}\left[\pi^{grid}(p_{d,t} - p_{d,t}^{sell}) + \pi^{gt,e} p_{d,t}^{gt} + \pi^{gt,h} h_{d,t}^{gt} + \pi^{gb} h_{d,t}^{gt}\right] \tag{8}$$

The coefficients πgrid, πgt,e , πgt,h , and πgb are the penalty factors used in the original program. They allow the dispatch model to internalize the environmental implications of grid electricity, CHP operation, and boiler heat production.

3.3 Energy-Conversion Relationships

The gas-turbine-based CHP unit converts natural gas into both electricity and heat. Let^{gt}g,t denote the gas flow consumed by the turbine. The power–heat output relationships are

$$p_{d,t}^{gt} = 0.3 H_g g_{d,t}^{gt},\ h_{d,t}^{gt} = 0.4 H_g g_{d,t}^{gt} \tag{9}$$

where Hg = 9.78 kWh/Nm3 is the lower heating value of natural gas. Equation (9) implies that the electricity-to-heat output ratio of the CHP unit is fixed, so the dispatch of the turbine simultaneously affects both the electric and thermal subsystems.

The ground source heat pump, electric chiller, and absorption chiller are modeled through fixed conversion coefficients:

$$h_{d,t}^{hp} = COP_{hp}\, p_{d,t}^{hp},\ c_{d,t}^{ec} = COP_{ec} p_{d,t}^{ec},\ c_{d,t}^{ac} = COP_{ac}\, h_{d,t}^{ac}, \tag{10}$$

with COPhp = 3.5, COPec = 4.2, and COPac = 1.2. The gas boiler is represented as

$$g_{d,t}^{gb} = \frac{h_{d,t}^{gb}}{\eta_{gb} H_g},\ \ \eta_{gb} = 0.9 \tag{11}$$

Accordingly, the total gas purchase from the external gas network is

$$g_{d,t}^{buy} = g_{d,t}^{gt} + g_{d,t}^{gb}. \tag{12}$$

3.4 Carrier-Balance Equations

The coordinated dispatch must satisfy the electricity, heat, and cooling balances at every hour. The electricity balance is

$$p_{d,t}^{buy} - p_{d,t}^{sell} + p_{d,t}^{pv} + p_{d,t}^{wt} + p_{d,t}^{gt} + p_{d,t}^{dis} - p_{d,t}^{ch} - p_{d,t}^{hp} - p_{d,t}^{ec} = p_{d,t}^{L} \tag{13}$$

which states that grid exchange, renewable generation, CHP electric output, and battery discharge must cover electric demand as well as the electricity consumption of storage charging, the ground source heat pump, and the electric chiller.

The heat balance is

$$h_{d,t}^{gt} + h_{d,t}^{hp} + h_{d,t}^{gb} + h_{d,t} - h_{d,t}^{ch} - h_{d,t}^{ac} = \widehat{H}_{d,t}^{L} \tag{14}$$

and the cooling balance is

$$c_{d,t}^{ee} + c_{d,t}^{ac} = \widehat{C}_{d,t}^{L}. \tag{15}$$

Equations (13)–(15) are the core coupling constraints of the integrated energy system because any change in device dispatch propagates across multiple carriers through the conversion relationships defined above.

3.5 Storage Dynamics and Exact Linear Logic

To improve mathematical transparency, the battery and thermal-storage subsystems are formulated with explicit energy-state variables rather than normalized state-of-charge variables. Let E^{e}s,t denote the battery energy state. The inter-temporal dynamics are

$$E_{d,t}^{es} = E_{d,t-1}^{es} + \eta_{es} P_{d,t} - \frac{1}{n_{es}} p_{d,t},\quad t = 1, \ldots, 24, \tag{16}$$

where ηes = 0.96. The energy-state and power limits are

$$0.1X_{es} \le E_{d,t}^{es} \le 0.9X_{es}, \tag{17}$$

$$0 \le p_{d,t}^{ch} \le 0.5X_{es}, 0 \le p_{d,t}^{dis} \le 0.5X_{es}. \tag{18}$$

The initial and terminal conditions enforce daily cycling consistency:

$$E_{d,0}^{es} = 0.55X_{es},\ E_{d,24}^{es} = 0.55X_{es}. \tag{19}$$

To exclude simultaneous charging and discharging, binary variables u^{ch}d, t and u^{dis}d, t are introduced:

$$p_{d,t}^{ch} \le 0.5X_{es},\quad p_{d,t}^{ch} \le 0.5\overline{X}_{es} u_{d,t}^{ch}, \tag{20}$$

$$p_{d,t}^{dis} \le 0.5X_{es},\quad p_{d,t}^{dis} \le 0.5\overline{X}_{es} u_{d,t}^{dis} \tag{21}$$

$$u_{d,t}^{ch} + u_{d,t}^{dis} \le 1,\ \ u_{d,t}^{ch}, u_{d,t}^{dis} \in \{0,1\}. \tag{22}$$

This reformulation is exact because the upper bound xes is known from the planning domain. When a binary state is zero, the corresponding charging or discharging power must also be zero; when the binary state is one, the admissible power is still restricted by the installed capacity xes.

The thermal-storage model is analogous. Let E^{h}ds,t denote the thermal energy state. Then

$$E_{d,t}^{hs} = E_{d,t-1}^{hs} + \eta_{hs} h_{d,t} - \frac{1}{\eta_{hs}} h_{d,t},\quad t = 1, \ldots, 24, \tag{23}$$

with ηhs =0.95, and

$$0.1X_{hs} \le E_{d,t}^{hs} \le 0.9X_{hs}, \tag{24}$$

$$0 \le h_{d,t}^{ch} \le 0.5X_{hs},\quad 0 \le h_{d,t}^{dis} \le 0.5X_{hs}, \tag{25}$$

$$E_{d,0}^{hs} = 0.55X_{hs},\ \ E_{d,24}^{hs} = 0.55X_{hs}. \tag{26}$$

The mutually exclusive charging/discharging logic is represented by

$$h_{d,t}^{ch} \le 0.5X_{hs},\quad h_{d,t}^{ch} \le 0.5\overline{X}_{hs} u_{d,t}^{h,ch}, \tag{27}$$

$$h_{d,t}^{dis} \le 0.5X_{hs},\quad h_{d,t}^{dis} \le 0.5\overline{X}_{hs} u_{d,t}^{h,dis}, \tag{28}$$

$$u_{d,t}^{h,ch} + u_{d,t}^{h,dis} \le 1,\ \ u_{d,t}^{h,ch}, u_{d,t}^{h,dis} \in \{0,1\}. \tag{29}$$

3.6 Technology Operating Limits

The renewable outputs are restricted by the exogenous availability profiles:

$$0 \le P_{d,t}^{pv} \le \alpha_{d,t}^{pv} X_{pv}, 0 \le p_{d,t}^{wt} \le \alpha_{d,t}^{wt} X_{wt}. \tag{30}$$

Bidirectional grid exchange is modeled through binary operating states:

$$0 \le p_{d,t}^{buy} \le \overline{P}^{grid} u_{d,t}^{buy}, \ \ 0 \le p_{d,t}^{sell} \le \overline{P}^{grid} u_{d,t} \tag{31}$$

$$u_{d,t}^{buy} + u_{d,t} \le 1, \ \ u_{d,t}^{buy}, u_{d,t}^{sell} \in \{0,1\}, \tag{32}$$

Where p^{-gird}= 500 kW is the maximum hourly grid-exchange limit used in the scheduling model.

The CHP unit must satisfy minimum-output and ramping constraints. Since xgt denotes the electric capacity of the gas turbine, the output bound is

$$p_{gt}^{min} \le p_{d,t} \le X_{gt}, \ \ p_{gt}^{min} = 20\,\text{kW}, \tag{33}$$

which is equivalently expressed in gas-flow form as

$$\frac{p_{gt}^{min}}{0.3H_g} \le g_{d,t}^{gt} \le \frac{X_{gt}}{0.3H_g}. \tag{34}$$

The hourly ramping constraint is

$$-40 \le p_{d,t}^{gt} - p_{d,t-1}^{gt} \le 40, \quad t = 2, \ldots, 24. \tag{35}$$

The remaining controllable devices are bounded by their installed capacities:

$$0 \le p_{d,t}^{hp} \le X_{hp}, 0 \le p_{d,t}^{ec} \le X_{ec} \tag{36}$$

$$0 \le h_{d,t}^{gb} \le X_{gb}, \quad 0 \le h_{d,t}^{ac} \le X_{ac}. \tag{37}$$

In the operational logic used in the program, the heat input of the absorption chiller is additionally limited by the CHP thermal output:

$$h_{d,t}^{ac} \le h_{d,t}^{gt}. \tag{38}$$

This constraint implies that absorption cooling is activated primarily when CHP heat is available, thereby strengthening the electricity–heat–cooling coupling structure of the system.

3.7 Equivalent Single-Level Milp Benchmark

Although the original implementation evaluates lower-level dispatch within a heuristic upper-level search, the complete planning–operation problem can be written as an equivalent single-level MILP benchmark:

$$\min_{X,\{y_d\}_{d=1}^{4}} C^{inv}(X) + \sum_{d=1}^{4} \omega_d \left(C_d^{dir} + C_d^{em}\right) \tag{39}$$

subject to (4)–(38) for all representative days and hours. This reformulation is exact under the present modeling assumptions because: (i) all investment terms are linear in installed capacities; (ii) all con- version relationships are linear; (iii) all time-coupled storage equations are linear; and (iv) the only capacity–logic interactions are represented by exact mixed-integer linear constraints using known upper bounds. Therefore, the MILP benchmark provides a deterministic reference solution against which the GA–PSO planning results can be checked.

3.8 Comprehensive Notation Summary

Table 1 summarizes the symbols used in the manuscript.

Table 1: Comprehensive notation table covering all variables used in the manuscript.

Symbol	Definition	Dimension / unit
	Sets and indices	
d	representative-day index	d = 1, . . . , 4
t	hourly index within one representative day	t = 1, . . . , 24
j	technology index	j ∈ {es, pv, wt, gt, hp, gb, hs, ac, ec}

Symbol	Definition	Dimension / unit
w_{d}	weight of representative day d	dimensionless
	Planning variables and bounds	
x_{es}	installed capacity of battery energy storage	kWh
x_{pv}	installed capacity of photovoltaic generation	kW
x_{wt}	installed capacity of wind generation	kW
x_{gt}	installed electric capacity of the CHP gas turbine	kW
x_{hp}	installed electrical capacity of the ground source heat pump	kW
x_{gb}	installed thermal capacity of the gas boiler	kW
x_{hs}	installed thermal-storage capacity	kWh
x_{ac}	installed heat-input capacity of the absorption chiller	kW
x_{ec}	installed electrical capacity of the electric chiller lower and upper planning	kW
$\underline{\boldsymbol{X}}_{\boldsymbol{j}}, \boldsymbol{X}_{\boldsymbol{j}}$	bounds of technology j	kW or kWh
	Exogenous profiles and prices	
$\hat{P}^{L}_{d,t}$	forecast electricity load at representative day d, hour t	kW
$\hat{H}^{L}_{d,t}$	forecast heat load at representative day d, hour t	kW
$\hat{C}^{L}_{d,t}$	forecast cooling load at representative day d, hour t	kW
$\hat{P}^{L}_{d,t}$	realized electricity load used in ex-post evaluation	kW
$\hat{H}^{L}_{d,t}$	realized heat load used in ex-post evaluation	kW
$\hat{C}^{L}_{d,t}$	realized cooling load used in ex-post evaluation	kW
$\hat{\partial}^{pv}_{d,t}$	available photovoltaic output factor	p.u.
$\hat{\partial}^{\mathrm{wt}}_{d,t}$	available wind output factor	p.u.
$\lambda^{\mathrm{e}}_{d,t}$	time-of-use electricity tariff	CNY/kWh
$\lambda^{\mathrm{g}}_{d,t}$	gas purchase price	CNY/Nm3
	Operational variables	
$P^{pv}_{d,t}$	scheduled photovoltaic output	kW
$P^{wt}_{d,t}$	scheduled wind output	kW
$P^{\mathrm{buy}}_{d,t}$	grid electricity purchase	kW
$P^{sell}_{d,t}$	grid electricity sale	kW
$\mathrm{u}^{\mathrm{buy}}_{d,t}$ $\mathrm{u}^{\mathrm{sell}}_{d,t}$	binary grid-trading states	{0, 1}

Symbol	Definition	Dimension / unit
$P_{d,t}^{ch}$ $P_{d,t}^{dis}$	battery charging and discharging power	kW
$u_{d,t}^{ch}$ $u_{d,t}^{dis}$	binary battery charging and discharging states	{0, 1}
$E_{d,t}^{es}$	battery energy state	kWh
$g_{d,t}^{gt}$	gas consumption of the CHP gas turbine	Nm^3/h
$p_{d,t}^{gt}$	thermal output of the CHP gas turbine	kW
$p_{d,t}^{hp}$	electric input of the ground source heat pump	kW
$h_{d,t}^{hp}$	heat output of the ground source heat pump	kW
$p_{d,t}^{ec}$	electric input of the electric chiller	kW
$c_{d,t}^{ec}$	cooling output of the electric chiller	kW
$h_{d,t}^{gb}$	heat output of the gas boiler	kW
$h_{d,t}^{ch}$ $h_{d,t}^{dis}$	thermal-storage charging and discharging power	kW
$u_{d,t}^{h,ch}$ $u_{d,t}^{h,dis}$	binary thermal-storage charging and discharging states	{0, 1}
$E_{d.t}^{hs}$	thermal-storage energy state	kWh
$h_{d.t}^{ac}$	heat input of the absorption chiller	kW
$c_{d,t}^{ac}$	cooling output of the absorption chiller	kW
$g_{d,t}^{gb}$	gas consumption of the gas boiler	Nm3/h
$g_{d,t}^{buy}$	total gas purchase	Nm3/h
	Model parameters and objective terms	
H_g	lower heating value of natural gas	9.78 kWh/Nm3
η_{es}	battery charging/discharging efficiency	0.96
η_{hs}	thermal-storage charging/discharging efficiency	0.95
η_{gb}	gas-boiler efficiency	0.9
COP_{hp}	coefficient of performance of the ground source heat pump	3.5
COP_{ec}	coefficient of performance of the electric chiller	4.2
COP_{ac}	coefficient of performance of the absorption chiller	1.2
c_j^{cop}	unit capital cost of technology j	CNY/kW or CNY/kWh
c_j^{om}	variable operation and maintenance cost of technology j	CNY/kWh
L_j	service life of technology j	year
r	discount rate	0.08

Symbol	Definition	Dimension / unit
CRF_j	capital recovery factor of technology j	dimensionless
π^{grid}	environmental penalty factor of grid electricity	penalty unit/kWh
$\pi^{gt,e}$, $\pi^{gt,h}$	environmental penalty factors of CHP electric and thermal output	penalty unit/kWh
π^{gb}	environmental penalty factor of boiler heat production	penalty unit/kWh
c^{inv}	daily equivalent annualized investment cost	CNY/day
c_d^{dir}	direct operating expenditure of representative day d	CNY/day
c_d^{em}	environmental penalty term of representative day d	penalty unit/day
Φ_d	optimal lower-level objective value on representative day d	composite unit/day
F	total planning–operation objective	composite unit

4. Solution Methodology

4.1 GA–PSO-Based Upper-Level Search

The upper-level planning problem is solved by a hybrid genetic algorithm and particle swarm optimization (GA–PSO) procedure. Let x_i^k and v_i^k denote the position and velocity of particle i at iteration k ,respectively. The standard PSO update is

$$\mathbf{v}_i^{k+1} = \omega \mathbf{v}_i^k + c_1 r_1 \left(\mathbf{p}_i^k - \mathbf{x}_i^k\right) + c_2 r_2 \left(\mathbf{g}^k - \mathbf{x}_i^k\right) \tag{40}$$

$$x_i^{k+1} = x_i^k + v_i^{k+1} \tag{41}$$

where p_i^k is the personal-best position of particle i, g k is the global-best position of the swarm, w is the inertia weight, c 1 and c2 are learning coefficients, and r1, r2 ~ U (0, 1) are independent random numbers.In the present study, each particle represents a candidate capacity vector X. For each candidate, the lower-level dispatch problem is solved on all representative days, and the resulting operating objective is combined with the investment term to evaluate the fitness value in (2). To strengthen global exploration, crossover and mutation operators are embedded after the PSO position update. Crossover recombines selected capacity coordinates from high-quality particles, while mutation randomly perturbs part of the population to prevent premature convergence. In the computational setting inherited from the original program, the population size is 20, the maximum number of iterations is 30, the inertia weight is 0.8, the two learning factors are both 0.5, the mutation rate is 0.05, and the crossover rate is 0.10.

4.2 Planning–Dispatch Evaluation Mechanism

The logic of the bilevel solution can be described as follows.

First, an initial population of feasible capacity vectors is generated within the planning bounds in (4). Second, for each candidate capacity vector, the day-ahead dispatch problem is solved over all representative days, subject to the full set of energy-balance, storage, and logical operating constraints. Third, the daily equivalent investment term and the weighted sum of representative-day operating terms are aggregated into a scalar fitness value. Fourth, the population is updated using the PSO velocity– position rules, followed by crossover and mutation. Fifth, infeasible particles are projected back into the admissible capacity domain. These steps are repeated until the stopping criterion is met, after which the best particle is reported as the heuristic planning solution.

This mechanism highlights the essential feature of the bilevel structure: the upper-level capacity decision is not evaluated through a simplified proxy objective, but through the exact day-ahead operation that the capacity mix induces. Therefore, the planning result already internalizes the temporal interaction among renewable generation, CHP operation, storage scheduling, grid exchange, and dual cooling technologies.

4.3 Role of the Exact Milp Benchmark

Although the heuristic GA–PSO framework is valuable for preserving the original engineering solution philosophy, a deterministic benchmark is useful for verifying the final planning outcome and for reporting a reproducible numerical optimum. The MILP benchmark in (39) serves exactly this purpose. Once the binary logical states are retained and all nonlinearities are replaced by exact mixed-integer linear relations, the integrated planning–operation problem becomes solvable by a commercial MILP solver. The benchmark therefore complements the heuristic search in two ways.

First, it provides a transparent and solver-independent mathematical statement of the entire model. Second, it allows the reported capacity configuration and cost values to be interpreted as the solution of a rigorously defined optimization problem rather than as the output of a black-box script. In this sense, the GA–PSO model and the MILP benchmark should not be viewed as competing formulations, but as two complementary representations of the same planning philosophy: the former mirrors the practical implementation process, whereas the latter improves theoretical clarity and reproducibility.

5. Case Study Settings

The numerical study uses four representative days with hourly electricity, heat, and cooling load forecasts, together with realized load trajectories for ex-post evaluation. The data package also provides hourly upper envelopes of photovoltaic and wind availability. The time-of-use electricity tariff ranges from 0.35 to 1.35 CNY/kWh, while the gas price ranges from 3.20 to 3.80 CNY/Nm3 . The planning bounds extracted from the code are summarized in Table 2.

Table 2: Planning bounds and optimal capacities.

Technology	Symbol	Lower	Upper	Optimal	Unit
Battery energy storage	x_{es}	400.00	800.00	800.00	kWh
Photovoltaic	x_{pv}	600.00	900.00	900.00	kW
Wind turbine	x_{wt}	400.00	600.00	600.00	kW
Gas turbine / CHP	x_{gt}	800.00	1200.00	1200.00	kW
Ground source heat pump	x_{hp}	300.00	500.00	300.00	kW
Gas boiler	x_{gb}	150.00	200.00	200.00	kW
Thermal storage	x_{hs}	400.00	600.00	600.00	kWh
Absorption chiller	x_{ac}	400.00	600.00	479.08	kW
Electric chiller	x_{ec}	100.00	150.00	150.00	kW

Table 3 lists the main techno-economic parameters used in planning and operation.

Table 3: Main techno-economic parameters.

Technology	Capex	Life	Capex unit	O&M	O&M unit
Battery energy storage	1500.00	10	CNY/kWh	0.0018	CNY/kWh
Photovoltaic	4800.00	20	CNY/kW	0.4	CNY/kWh
Wind turbine	6000.00	15	CNY/kW	0.9	CNY/kWh
Gas turbine / CHP	7900.00	15	CNY/kW	0.007	CNY/kWh
Ground source heat pump	1050.00	20	CNY/kW	0.026	CNY/kWh
Gas boiler	900.00	15	CNY/kW	0.0082	CNY/kWh
Thermal storage	150.00	10	CNY/kWh	0.0015	CNY/kWh
Absorption chiller	1200.00	15	CNY/kW	0.03	CNY/kWh
Electric chiller	800.00	15	CNY/kW	0.08	CNY/kWh

The prediction accuracy of the three demand carriers is summarized in Table 4. The mean absolute percentage error remains around 5%, indicating that the forecasts are sufficiently accurate for day-ahead coordination while still leaving non-negligible deviation for ex-post assessment.

Table 4: Forecast-error statistics of the representative-day demand data.

Load type	MAE	RMSE	MAPE (%)
Electricity	29.88	35.86	4.92
Heat	20.12	27.07	4.64
Cooling	22.24	29.75	5.02

Figure 1 shows the representative-day renewable availability, and Figures 2–4 compare the forecast and realized demand profiles.

Figure 1: Representative-day wind and photovoltaic availability profiles.

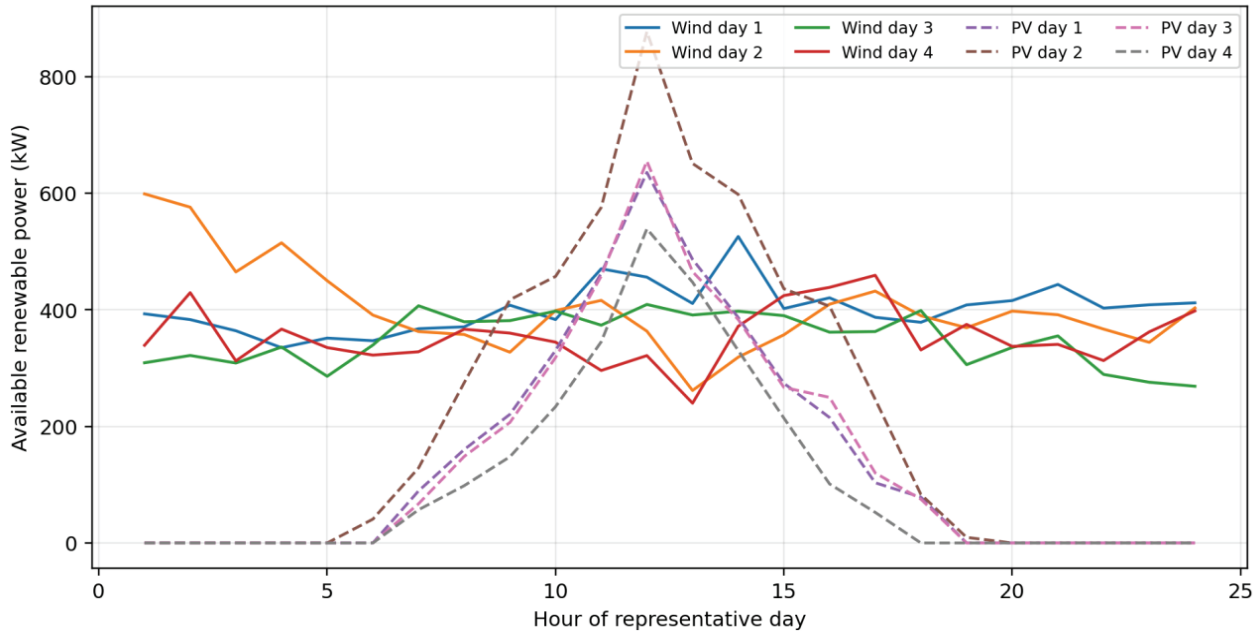

Figure 2: Forecast and realized electricity loads.

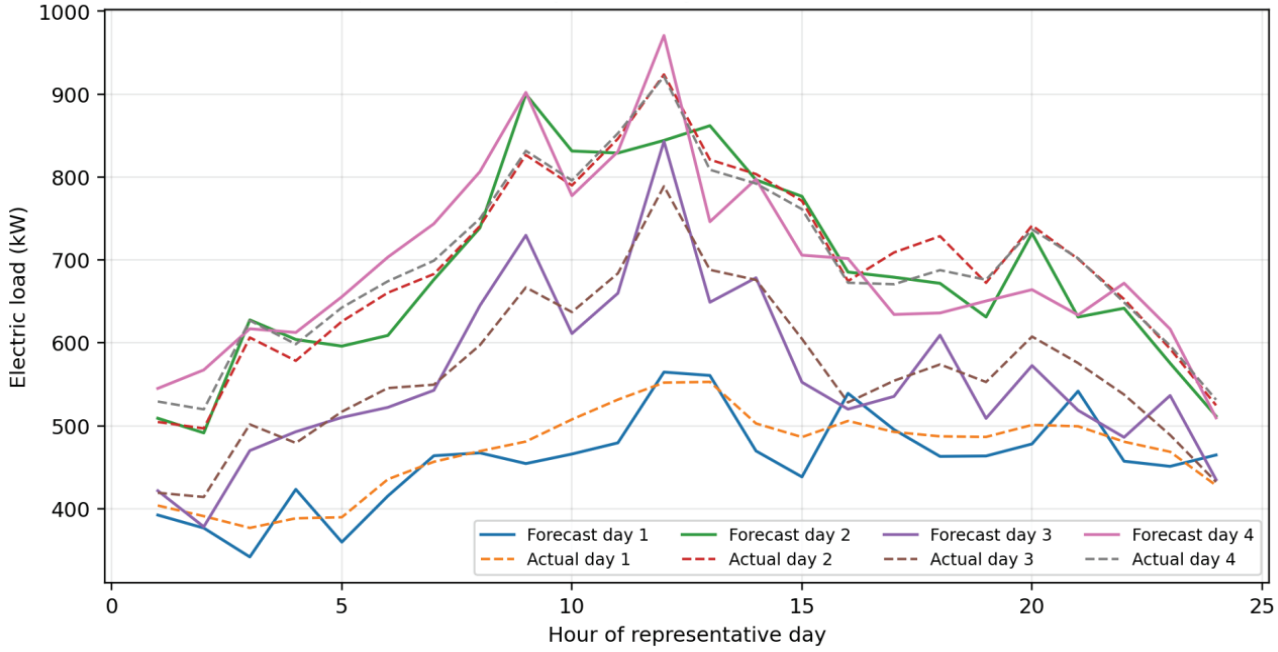

Figure 3: Forecast and realized heat loads.

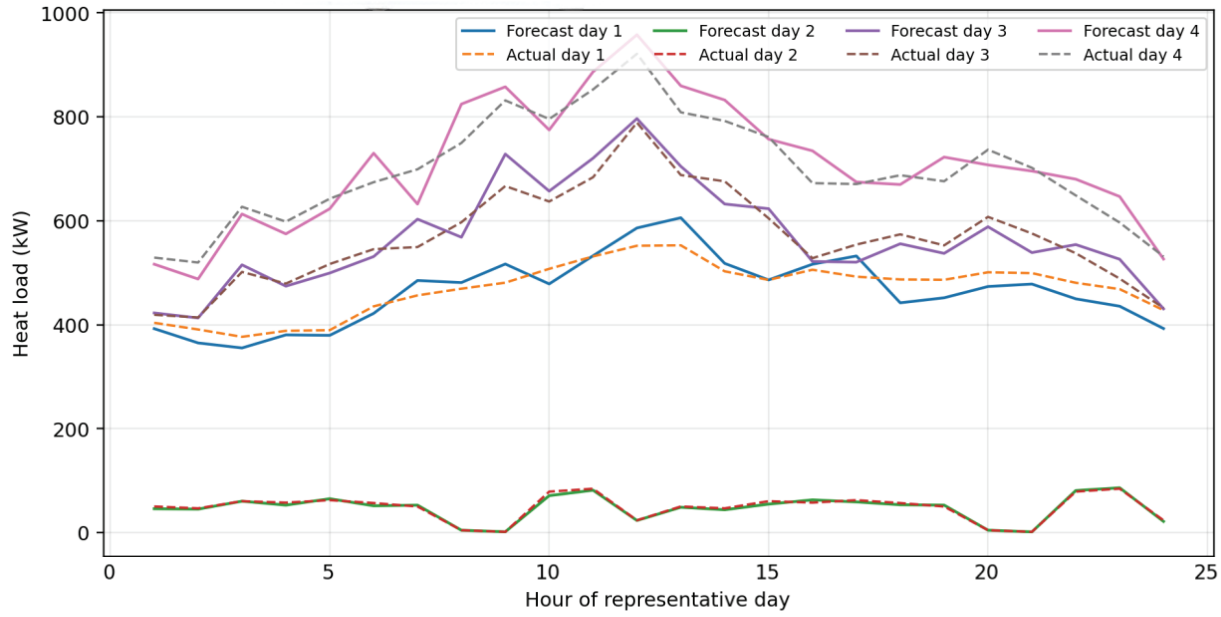

Figure 4: Forecast and realized cooling loads.

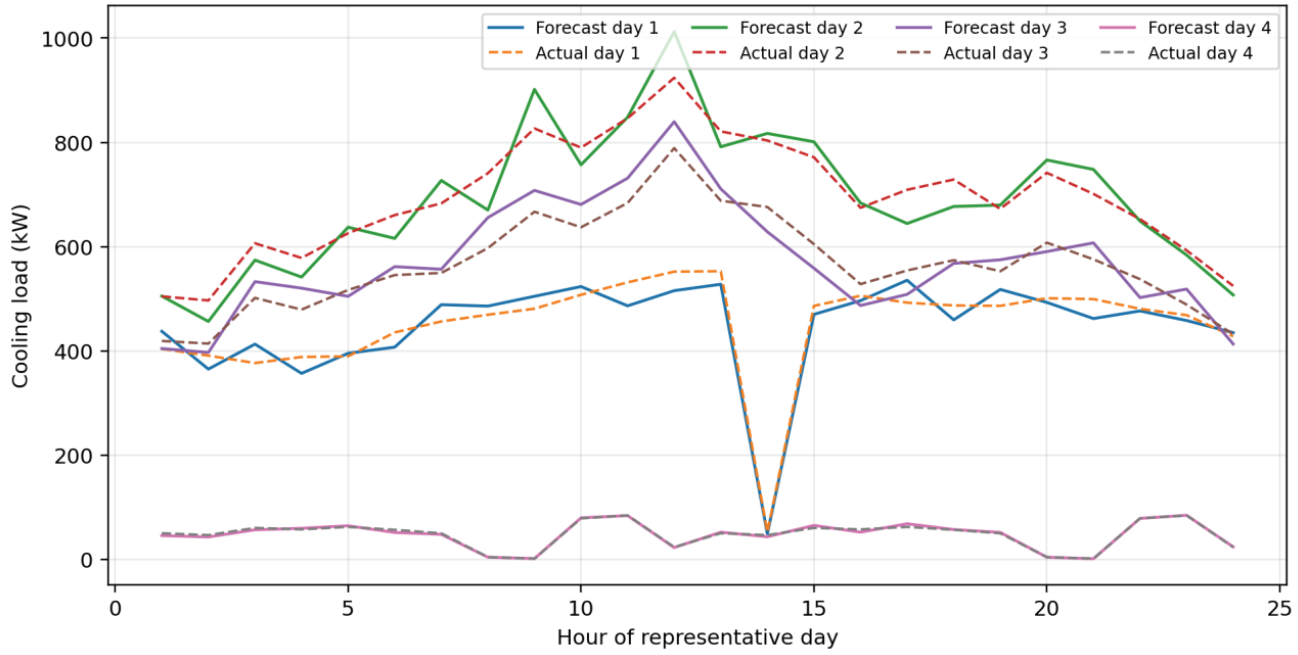

6. Results and Discussion

6.1 Optimal Capacity Configuration

The optimal capacity mix obtained from the benchmark model is reported in Table 2 and illustrated in Figure 5. Several structural features are noteworthy. First, the capacities of photovoltaic generation, wind generation, battery storage, the gas turbine, thermal storage, and the electric chiller all reach the upper bounds of their admissible planning intervals. This result indicates that, under the present demand patterns and price structure, renewable penetration and multi-timescale flexibility provide substantial system value. Second, the ground source heat pump is selected at its lower bound, suggesting that heat supply from CHP and auxiliary heating already satisfies most thermal requirements cost-effectively. Third, the absorption chiller converges to an interior optimum of 479.08 kW rather than to a boundary solution, which implies that the cooling structure is determined by a nontrivial temporal trade-off between electricity-driven and heat-driven refrigeration.

Figure 5: Optimal capacity configuration of the integrated energy system.

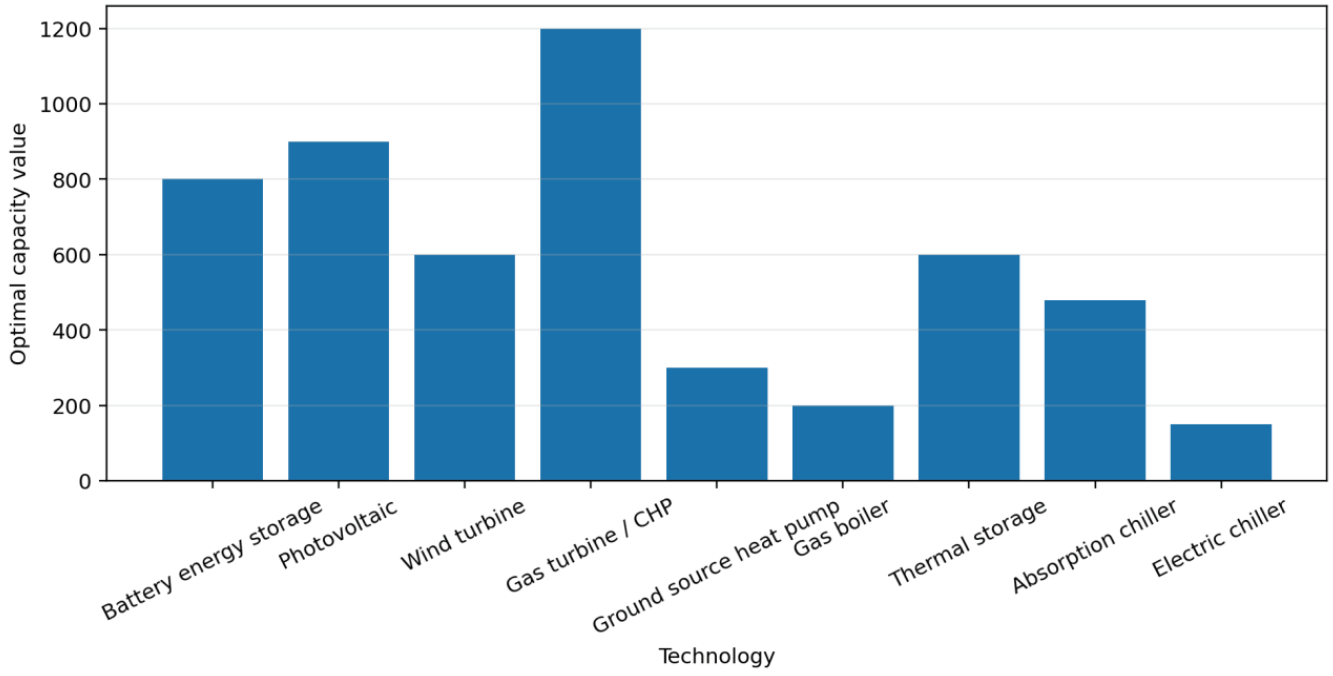

The daily equivalent annualized investment cost is 6286.79. Among all technologies, the CHP unit contributes the largest share to the investment term, followed by photovoltaic and wind generation. This ranking is consistent with the relatively high unit capital cost of the gas turbine and the large renewable capacities selected by the optimization.

6.2 Representative-Day Dispatch Characteristics

Table 5 summarizes the main load and supply quantities on each representative day. Representative days 2 and 4 are the most electricity-intensive, while representative day 4 also exhibits the highest heat demand. Representative day 2 is dominated by cooling demand, which activates both the electric chiller and the absorption chiller. By contrast, representative day 4 is primarily heat-driven and has only limited cooling demand.

Table 5: Representative-day load and supply summary.

Day	Ele. load	Heat load	Cool load	WT	PV	Grid buy	Grid sell
1	11028.10	11160.51	10763.60	9648.71	3443.96	1744.54	5409.76
2	16452.60	1130.65	16596.38	9666.06	5203.46	1939.58	4040.73
3	13429.73	13665.97	13761.85	8383.59	3414.35	3515.05	3503.67
4	16700.50	16988.81	1150.91	8514.85	2566.94	4422.79	2363.67

The dispatch profiles in Figures 6–8 reveal the internal coordination mechanism of the system. On representative day 2, strong wind and photovoltaic generation reduce net grid dependence during several hours, while the electric chiller and the ground source heat pump increase electrical demand in response to the high cooling load. At the same time, the CHP unit supplies recoverable heat that can be converted into cooling by the absorption chiller, thereby partially shifting the cooling burden away from the electrical side. On representative day 4, the thermal subsystem becomes the dominant operational focus: CHP heat, the ground source heat pump, the gas boiler, and thermal storage jointly satisfy the high heating requirement. These results demonstrate that the value of an integrated energy system does not arise merely from technology coexistence, but from the ability to redirect energy between carriers according to hourly marginal conditions.

Figure 6: Representative day 2 electric dispatch profile.

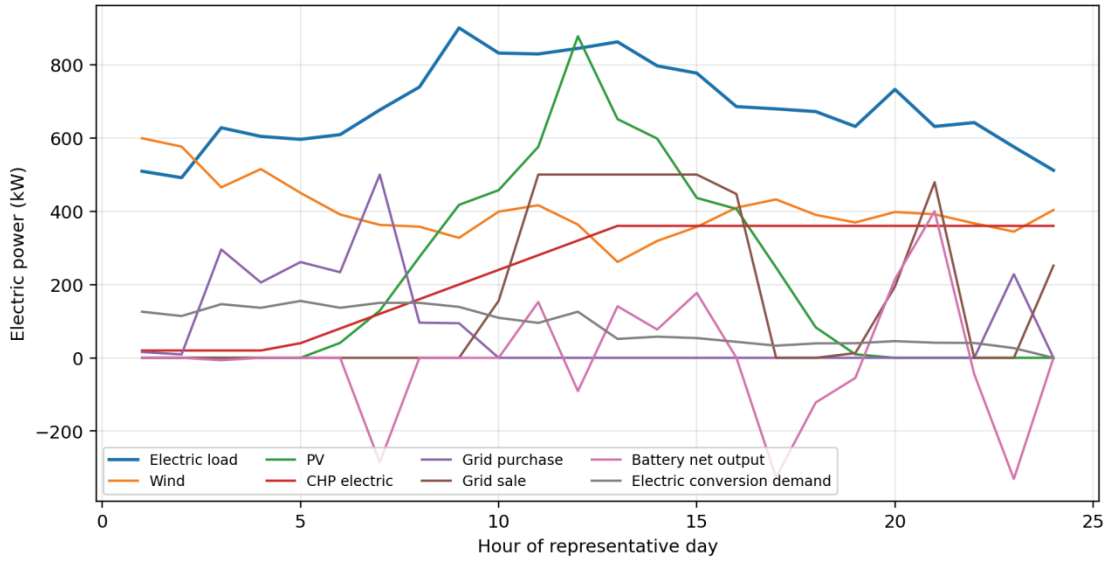

Figure 7: Representative day 4 heat dispatch profile.

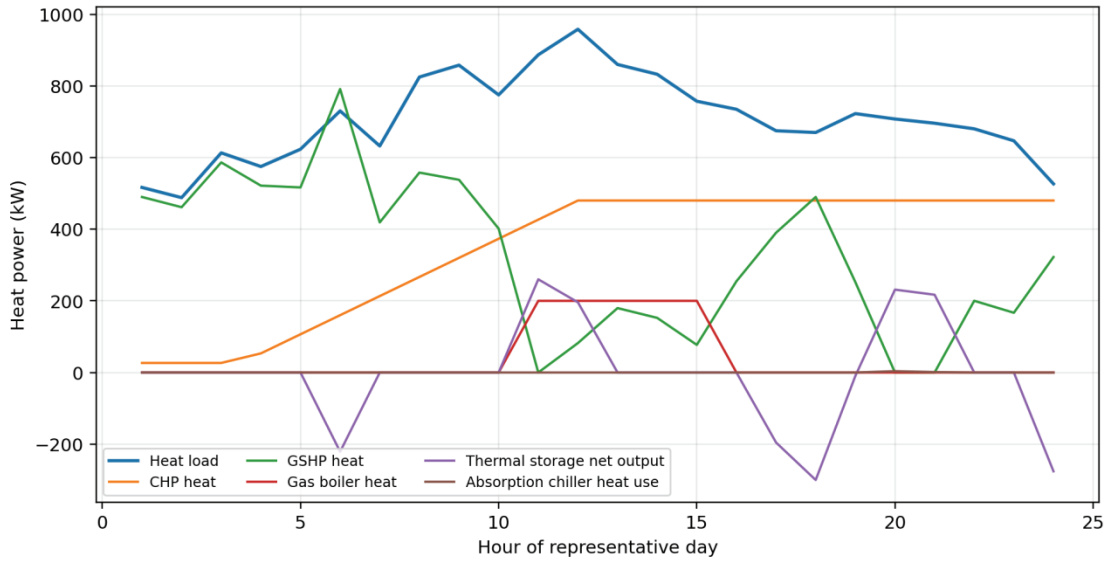

Figure 8: Representative day 2 cooling dispatch profile.

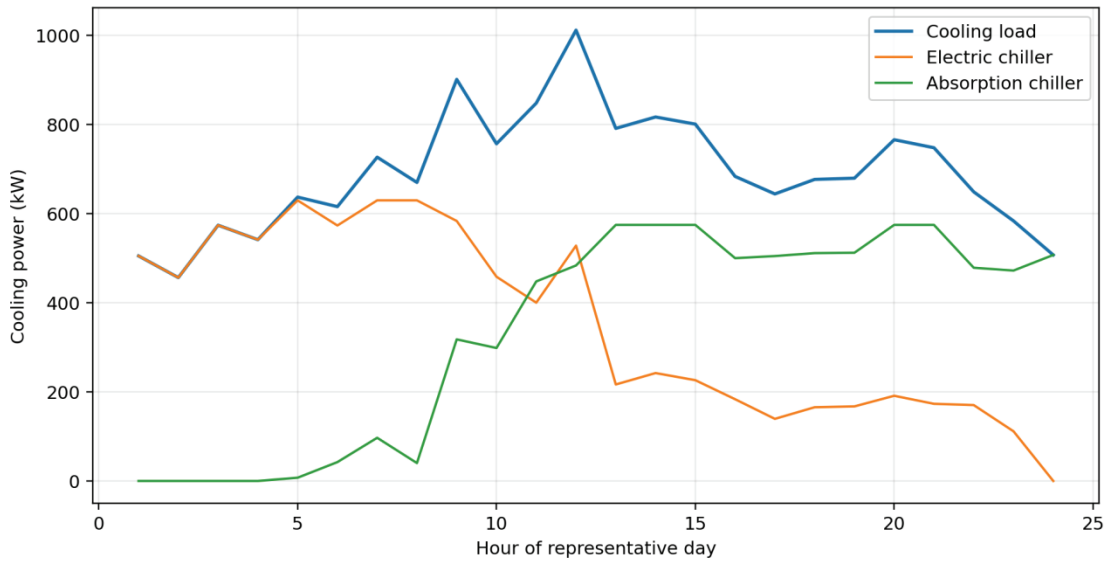

6.3 Economic and Ex-Post Operating Performance

Table 6 reports the forecast and realized operating results of each representative day. The total day- ahead composite operating objective over the four representative days is 77400.43, whereas the ex-post composite operating objective under realized loads is 78763.31. The increase is moderate, indicating that the selected capacity mix and dispatch structure remain robust under forecast deviation. The complete planning–operation objective, including the daily equivalent annualized investment term, is 83687.21.

Table 6: Representative-day operating results.

Day	F. direct	F. emission	F. comp.	A. direct	A. emission	A. comp.
1	11294.67	2024.31	13318.98	11615.95	2379.45	13995.39
2	14125.36	4159.39	18284.75	14383.25	4418.56	18801.81
3	14225.49	7028.15	21253.64	14410.05	7192.17	21602.22
4	15444.79	9098.28	24543.07	15450.34	8913.54	24363.88

Several insights can be drawn from these results. First, available renewable power is effectively utilized because it directly reduces grid purchases and weakens the environmental penalty associated with external electricity supply. Second, the CHP unit acts as a structural anchor of the system by simultaneously supporting the electricity and heat balances and by enabling absorption cooling through recoverable heat. Third, the joint presence of battery storage and thermal storage improves temporal flexibility on both the electrical and thermal sides, allowing the system to shift energy across hours and to mitigate part of the mismatch between renewable availability and demand. Fourth, the coexistence of the electric chiller and the absorption chiller allows the cooling load to be allocated dynamically between electricity and heat, which is particularly valuable when renewable output, CHP heat availability, and grid prices vary significantly across the day.

From an ex-post perspective, the gap between the forecast and realized objectives is mainly attributable to additional electricity purchase and compensatory thermal production when realized load exceeds the forecast level. Nevertheless, the deviation remains limited, which suggests that the optimized capacity portfolio provides adequate flexibility for representative forecast error levels.

7. Conclusion

This paper presents a complete reformulation of a bilevel integrated energy system model for coordinated capacity planning and day-ahead scheduling. The upper level determines the capacities of renewable generation, conversion devices, and storage technologies, while the lower level coordinates electricity, heat, cooling, and gas flows over representative days. The model explicitly represents renewable generation, CHP coupling, heating and cooling conversion, bidirectional grid interaction, storage dynamics, and gas consumption, and it is supported by a unified notation system and a detailed parameter specification.

To improve both interpretability and reproducibility, the study retains the original GA–PSO planning philosophy and further establishes an equivalent mixed-integer linear benchmark model. The numerical results show that the optimal configuration favors strong renewable deployment together with relatively large CHP, battery, and thermal-storage capacities. The representative-day dispatch results further demonstrate that coordinated use of CHP, heat pumping, electricity-driven cooling, and heat-driven cooling can effectively manage the multi-carrier demand structure. Overall, the study confirms that bilevel planning with explicit electricity–heat–cooling coupling provides an effective framework for the design and operation of integrated energy systems with renewable uncertainty and interdependent conversion technologies.

Funding

No

Conflict of Interests

The authors declare that there is no conflict of interest regarding the publication of this paper.

Reference

[1] M. Geidl, G. Koeppel, P. Favre-Perrod, B. Kloeckl, G. Andersson, and K. Froehlich, “Energy hubs for the future,” IEEE Power & Energy Magazine, vol. 5, no. 1, pp. 24–30, 2007.

[2] M. Geidl and G. Andersson, “Optimal power flow of multiple energy carriers,” IEEE Transactions on Power Systems, vol. 22, no. 1, pp. 145–155, 2007.

[3] G. Chicco and P. Mancarella, “Distributed multi-generation: A comprehensive view,” Renewable and Sustainable Energy Reviews, vol. 13, no. 3, pp. 535–551, 2009.

[4] C. Marnay, G. Venkataramanan, M. Stadler, A. S. Siddiqui, R. Firestone, and B. Chandran, “Optimal technology selection and operation of commercial-building microgrids,” IEEE Transactions on Power Systems, vol. 23, no. 3, pp. 975–982, 2008.

[5] E. Fabrizio, V. Corrado, and M. Filippi, “A model to design and optimize multi-energy systems in buildings at the design concept stage,” Renewable Energy, vol. 35, no. 3, pp. 644–655, 2010.

[6] J. Keirstead, M. Jennings, and A. Sivakumar, “A review of urban energy system models: Ap- proaches, challenges and opportunities,” Renewable and Sustainable Energy Reviews, vol. 16, no. 6, pp. 3847–3866, 2012.

[7] S. Pfenninger, A. Hawkes, and J. Keirstead, “Energy systems modeling for twenty-first century energy challenges,” Renewable and Sustainable Energy Reviews, vol. 33, pp. 74–86, 2014.

[8] P. Mancarella, “MES (multi-energy systems): An overview of concepts and evaluation models,” Energy, vol. 65, pp. 1–17, 2014.

[9] J. Wu, J. Yan, H. Jia, N. Hatziargyriou, N. Djilali, and H. Sun, “Integrated energy systems,” Applied Energy, vol. 167, pp. 155–157, 2016.

[10] J. Reynolds, M. Ahmad, and Y. Rezgui, “Holistic modelling techniques for the operational optimi- sation of multi-vector energy systems,” Energy and Buildings, vol. 169, pp. 397–416, 2018.

[11] R. Rigo-Mariani, S. O. C. Wae, S. Mazzoni, and A. Romagnoli, "Comparison of optimization frameworks for the design of a multi-energy microgrid," Applied Energy, vol. 257, p. 113982, 2020.

[12] S. A. Mansouri, A. Ahmarinejad, M. Ansarian, M. S. Javadi, and J. P. S. Catalao, “Stochastic planning and operation of energy hubs considering demand response programs using Benders decomposition approach,” International Journal of Electrical Power & Energy Systems, vol. 120, p. 106030, 2020.

[13] A. E. H. Berjawi, S. L. Walker, C. Patsios, and S. H. R. Hosseini, "An evaluation framework for future integrated energy systems: A whole energy systems approach," Renewable and Sustainable Energy Reviews, vol. 145, p. 111163, 2021.

[14] M. H. Shams, M. Shahabi, M. MansourLakouraj, M. Shafie-khah, and J. P. S. Catalao, "Adjustable robust optimization approach for two-stage operation of energy hub-based microgrids," Energy, vol. 222, p. 119894, 2021.

[15] P. C. Taylor, M. Abeysekera, Y. Bian, D. Cetenovic, M. Deakin, A. Ehsan, V. Levi, F. Li, R. Oduro, R. Preece, P. G. Taylor, V. Terzija, S. L. Walker, and J. Wu, “An interdisciplinary research perspective on the future of multi-vector energy networks,” International Journal of Electrical Power & Energy Systems, vol. 135, p. 107492, 2022.

[16] T. Ding, W. Jia, M. Shahidehpour, O. Han, Y. Sun, and Z. Zhang, “Review of optimization methods for energy hub planning, operation, trading, and control,” IEEE Transactions on Sustainable Energy, vol. 13, no. 3, pp. 1802–1818, 2022.

[17] Y. Zhou, X. Li, H. Han, Z. Wei, H. Zang, G. Sun, and S. Chen, "Resilience-oriented planning of integrated electricity and heat systems: A stochastic distributionally robust optimization approach," Applied Energy, vol. 353, p. 122053, 2024.

[18] X. Wu, B. Zhang, M. P. Nielsen, and Z. Chen, "Multi-stage planning of integrated electricity-gas-heating system in the context of carbon emission reduction," Applied Energy, vol. 358, p. 122584, 2024.

[19] J. H. Holland, Adaptation in Natural and Artificial Systems. Ann Arbor, MI, USA: University of Michigan Press, 1975.

[20] J. Kennedy and R. Eberhart, “Particle swarm optimization,” in Proceedings of the IEEE Interna- tional Conference on Neural Networks, 1995, pp. 1942–1948.

[21] J. Lofberg, “YALMIP: A toolbox for modeling and optimization in MATLAB,” in Proceedings of the CACSD Conference, Taipei, Taiwan, 2004, pp. 284–289.

[22] Gurobi Optimization, LLC, Gurobi Optimizer Reference Manual. Beaverton, OR, USA, 2024.